Journal of Materials Chemistry

Dynamic Article Links

Cite this: DOI: 10.1039/c1jm12820e

www.rsc.org/materials

PAPER

Optical and electrical properties of efficiency enhanced polymer solar cells with Au nanoparticles in a PEDOT–PSS layer†

Dixon D. S. Fung,[a] Linfang Qiao,[ab] Wallace C. H. Choy,*[a] Chuandao Wang,[a] Wei E. I. Sha,[a] Fengxian Xie[a] and Sailing He[ab]

Received 19th June 2011, Accepted 8th August 2011
DOI: 10.1039/c1jm12820e

We unveil new device physics and provide details of device mechanisms by investigating polymer solar cells (PSCs) incorporating Au nanoparticles (NPs) into the hole collection poly(3,4-ethylenedioxythiophene) poly(styrenesulfonate) (PEDOT:PSS) layer. Theoretical and experimental results show that the very strong near field around Au NPs due to Localized Surface Plasmonic Resonance (LSPR) mainly distributes laterally along the PEDOT:PSS layer rather than vertically into the adjacent active layer, leading to minimal enhancement of light absorption in the active layer. This finding can be extended to a typical class of solar cells incorporating metallic NPs in spacing layers adjacent to the active layer. With optical effects proven to be minor contributors to device performance improvements, we investigate the electrical properties of the PSCs and obtain insights into the detailed device mechanisms. Improvements in power conversion efficiency (PCE) of solar cells are found to originate from the enlarged active layer/PEDOT:PSS interfacial area and improved PEDOT:PSS conductivity. At high NP concentrations, reduced exciton quenching at donor/acceptor junctions is found to cause PCE deterioration. Our findings indicate that it is highly important to investigate both optical and electrical effects for understanding and optimizing PSC performances.

1. Introduction

Amongst various emerging technologies in the field of photovoltaics, the bulk-heterojunction polymer solar cells (PSCs) have proved to be highly promising candidates, due to their simple fabrication procedure, physical flexibility and low material cost.[1] However, there are still some challenges to address in organic photovoltaics. In particular, the low exciton diffusion length and low carrier mobility of organic semiconductors[2–6] limit the light absorption efficiency and thereby the power conversion efficiency (PCE) in such cells. Efforts have been made to cater for this problem. One method of particular interest is the incorporation of metallic nanoparticles (NPs), commonly Au or Ag NPs, into device structures. By utilizing the Localized Surface Plasmon Resonance (LSPR) effect, electromagnetic fields near metallic NPs can theoretically be enhanced for improving the optical absorption in PSCs.[7–12]

Although efficiency enhancements in PSCs through the incorporation of NPs have been investigated experimentally,[13–21] the degree of contribution of LSPR effects remains inconclusive. Limitations exist in using incident photon to electron conversion efficiency (IPCE) as the evidence for LSPR effects, as IPCE is highly affected by the electrical characteristics of the devices. Furthermore, if LSPR effects are present, it is still uncertain whether the enhancement of the electromagnetic fields near metallic NPs can improve the light absorption in the active layer. Meanwhile, some reports have stated that the variation of solar cell performances may be due to the introduction of 'dopant states' in the active layer or modified electrode interfaces.[22,23] It has also been shown that additives can induce morphological changes in the PEDOT:PSS layer.[24,25] Consequently, the investigation of both electrical and optical effects is highly important and desirable to better understand the actual physics within the 'plasmonic' PSC.

To investigate the origin of performance improvement after addition of NPs, we study the effect of doping the PEDOT:PSS layer of a PSC with ~18 nm diameter Au NPs. Monofunctional poly(ethylene glycol) (PEG)-capped Au NPs are doped into the PEDOT:PSS hole collection layer of an optimized PSC with poly (3-hexylthiophene) (P3HT):phenyl-C61-butyric acid methyl ester (PCBM) as the active layer, leading to ~13% peak PCE improvement. The effect of PEG capping on Au NPs is also investigated from a device fabrication perspective. Together with

[a]Department of Electrical and Electronic Engineering, University of Hong Kong, Pokfulam Road, Hong Kong, China. E-mail: chchoy@eee.hku.hk; Fax: +852-2559-8738; Tel: +852-2587-8485
[b]Centre for Optical and Electromagnetic Research, State Key Laboratory of Modern Optical Instrumentations, Zhejiang University, Hangzhou, 310058, China

† Electronic supplementary information (ESI) available: The theoretical model for optical simulation, supplementary figures of *J–V* curves for double layer PEDOT:PSS devices and AFM of the P3HT:PCBM top surface. See DOI: 10.1039/c1jm12820e

theoretical simulations, we investigate the impact of Au NPs on the optical and electrical properties of our PSCs. Our results show that the competition between improved hole collection at the PEDOT:PSS/active layer interface and reduced exciton quenching, at donor/acceptor junctions, instead of the LSPR effect, is a major contributor to the measured PCE variation.

2. Experimental

2.1 Synthesis of Au NPs

The synthesis method for Au NPs was reported previously.[26,27] To cap the Au NPs with PEG, 10 mg of *O*-[2-(3-mercaptopropionylamino)ethyl]-*O*′-methylpolyethylene glycol (M_w 5000, Sigma-Aldrich) was dissolved in 1 ml of deionized water, and then the solution was rotated in a rotary evaporator to make it uniform. 0.5 ml of Au NPs was added into the solution and then heated at 70 °C for 15 minutes to evaporate the water. The NPs are then dissolved in 0.5 ml of deionized water to make a uniform solution.

2.2 Device fabrication and characterization

To prepare different concentrations of Au NPs in PEDOT:PSS layers, 20 μl of Au NP solution of various NP concentrations is added to 80 μL of PEDOT:PSS (Baytron AI 4083). The resulting solutions were spin-coated onto ITO-coated glass substrates and were subsequently annealed at 140 °C for 10 min. The resulting thickness of PEDOT:PSS is ~30 nm measured by a Dektak stylus profiler. Incorporation of Au NPs does not alter the PEDOT:PSS film thickness. For devices with an additional layer of PEDOT:PSS fabricated on top of the PEDOT:PSS:Au NP layer, the PEDOT:PSS:Au NP films were treated by ultraviolet light for 1 min. PEDOT:PSS was then spin-coated on top of the layer and then annealed for 10 min. The active layer comprises P3HT (Luminescence Technology Corp.) and PCBM (Nichem Fine Technology Ltd.). The polymer blend solution was prepared by mixing P3HT and PCBM at 1 : 1 ratio, with a total concentration of 45 mg ml^{-1}. Device fabrication conditions were optimized prior to this investigation. The mixed solution was spin-coated at 800 rpm for 45 seconds, and was then subjected to solvent annealing for ~40 min. The film was then thermally annealed at 110 °C for 10 min. The thickness of the active layer is ~220 nm. Finally, LiF (1 nm) and Al (100 nm) are sequentially evaporated onto the polymer layer as a cathode to create a device of area 5.77 mm^2 defined by a shadow mask.

The transmission electron microscope (TEM) image of Au NPs was measured using a Philips Tecnai G2 20 S-TWIN. Scanning Electron Microscope (SEM) images are measured using a Hitachi F-4800 FEG SEM. The absolute refractive index and absorption coefficient were measured by the spectroscopic ellipsometry (Woollam). Details of the measurement of *J*–*V* characteristics have been described elsewhere.[28] The IPCE measurement was performed by a system combining xenon lamp, a monochromator, a chopper and a lock-in amplifier together with a calibrated silicon photodetector (Hamamatsu mono-Si cell). AFM characterization was conducted by using an Asylum Research MFP-3D in tapping mode.

2.3 Theoretical modeling

The effects of Au NPs on the light absorption at the active layer of organic solar cells and thus the exciton generation rate have been theoretically determined. As a rigorous, fast and efficient solver of Maxwell's equation, volume integral equation-fast Fourier transform (VIE-FFT) has been built in this work. The algorithm is particularly capable of modeling thin-film solar cells incorporating small plasmonic NPs of sizes ranging from 10 nm to 100 nm. The plasmon coupling and hybridization of metallic NPs, as well as their interplay with the solar cell device structure, have been fully taken into account. Details of the model are described in ESI A†.

3. Results and discussion

3.1 Device performances for Au NP devices

The current density (*J*) *versus* voltage (*V*) characteristics of devices with structure ITO/PEDOT:PSS (with PEG-capped Au NPs)/P3HT:PCBM/LiF (1 nm)/Al (100 nm) incorporating various Au NP concentrations in the PEDOT:PSS layer are shown in Fig. 1. The device characteristics are summarized in Table 1. We can observe that increasing Au NP concentration in PEDOT:PSS improves PCE of our PSCs, peaking at 0.32 wt% with a PCE of 3.51% which corresponds to ~13% improvement. Improvements originate from increases in FF and J_{sc}, from 0.58 to 0.62 and 8.5 mA cm^{-2} to 8.94 mA cm^{-2}, respectively. Further increasing the concentration of NPs has detrimental effect on device performances, with PCE dropping to 2.80% at 1.92 wt% Au NP concentration. From the dark *J*–*V* characteristics in the inset of Fig. 1, no significant change in the leakage current is observed after incorporation of Au NPs. In order to understand the underlying physics of the PCE trend, we study the optical and electrical properties of our devices in the following sections.

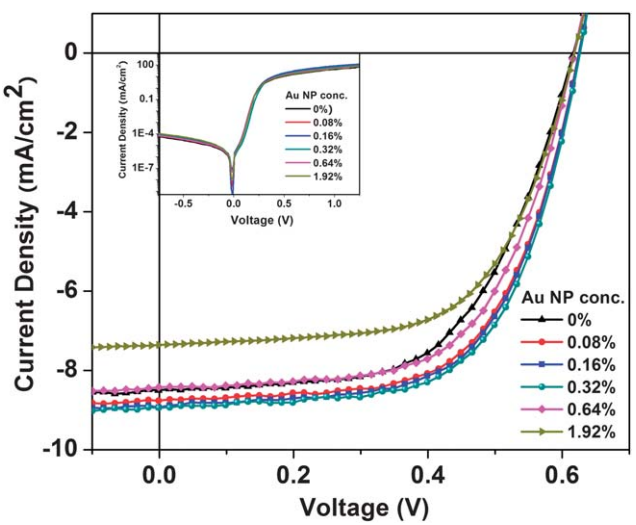

Fig. 1 *J*–*V* characteristics of solar cells with structure ITO/PEDOT:PSS (with PEG-capped Au NPs)/P3HT:PCBM/LiF (1 nm)/Al (100 nm), incorporated with different NP concentrations under AM 1.5G illumination at 100 mW cm^{-2}. Inset: dark *J*–*V* characteristics of the solar cells.

Table 1 Device performances for solar cells with structure ITO/PEDOT:PSS (with PEG-capped Au NPs)/P3HT:PCBM/LiF (1 nm)/Al (100 nm), incorporated with different NP concentrations

NP concentration (wt %)	J_{sc}/ mA cm^{-2}	V_{oc}/V	FF (%)	PCE (%)
0	8.5 ± 0.19	0.62 ± 0.01	58 ± 1.3	3.10 ± 0.10
0.08	8.77 ± 0.23	0.63 ± 0.01	61 ± 1.0	3.40 ± 0.11
0.16	8.93 ± 0.19	0.63 ± 0.01	61 ± 1.1	3.46 ± 0.10
0.32	8.94 ± 0.15	0.63 ± 0.01	62 ± 1.0	3.51 ± 0.09
0.64	8.56 ± 0.11	0.62 ± 0.01	61 ± 1.2	3.21 ± 0.10
1.92	7.36 ± 0.2	0.62 ± 0.01	61 ± 0.5	2.80 ± 0.13

3.2 Au NP properties and the effects of PEG

The absorption spectrum of Au NPs without PEG in water is shown in Fig. 2. The absorption peak at ~520 nm corresponds to the excitation of LSPR. Coating PEG onto Au NPs has no discernible effect on the peak position of optical absorption. The average diameter of Au NPs is approximately 18 nm, based on Transmission Electron Microscope (TEM) measurements, as shown in the inset of Fig. 2.

Both types of Au NPs, with or without PEG coating, are mixed with PEDOT:PSS solution in water, and a device of structure ITO/PEDOT:PSS:Au NPs/P3HT:PCBM/LiF (1 nm)/Al (100 nm) was fabricated to investigate the device performance. For the same concentration (0.32 wt%) of Au NPs, PCE of the device with Au NP (PEG) improves from 3.1% (control) to 3.51%, while devices with Au NP (no PEG) show no performance improvement. To investigate the origin of this effect, Scanning Electron Microscope (SEM) images were taken on PEDOT:PSS:Au NP films. As shown in Fig. 3a, Au NPs with PEG are well dispersed in a PEDOT:PSS:Au NP film with no clear aggregation, while Au NPs without PEG aggregate into clumps of NPs in a film (Fig. 3b). Our synthesis method produces Au NPs with a positive surface charge,[26] while PSS molecules are anionic in nature.[29] When Au NPs are added to PEDOT:PSS solution, the adsorption of anionic PSS molecules on positively charged Au NPs leads to the aggregation of Au NPs. On the other hand, the PEG capping layer has a shielding effect on Au NPs, leading to reduced interaction of NPs with the surrounding medium.[30] To make sure that PEG itself does not have any effect other than the prevention of Au NP aggregation,[27] we compared devices with and without PEG (2 mg ml^{-1}) dissolved into the PEDOT:PSS layer and observed no discernible difference in the performance. Therefore, PEG itself does not exert any significant effects on our device performances. The contribution of PEG is to prevent formation of aggregation sites and allow the uniform dispersion of Au NPs. Hence, we will investigate the effects of PEG-capped Au NPs on PSCs, and all mentions of Au NPs are considered to be PEG-capped hereafter in this report.

The positioning of Au NPs along the vertical profile of the PEDOT:PSS film is shown in Fig. 3c. It can be observed that the majority of the bulk of individual NPs are located within the PEDOT:PSS layer. At the locations of Au NPs, bumps are created on the surface of PEDOT:PSS. However, it should be noted that the Au NPs at the bumps are still covered by a layer of PEDOT:PSS and we did not observe any bare Au NP protrusions in our measurements.

3.3 Plasmonic effects

In order to directly investigate LSPR effects, we measured the absorption spectrum of the PEDOT:PSS/P3HT:PCBM films, with or without Au NPs in PEDOT:PSS as shown in Fig. 4a. Interestingly, we observed no significant difference in absorption between the samples with and without Au NPs. In order to understand plasmonic effects of Au NPs in the devices, we have

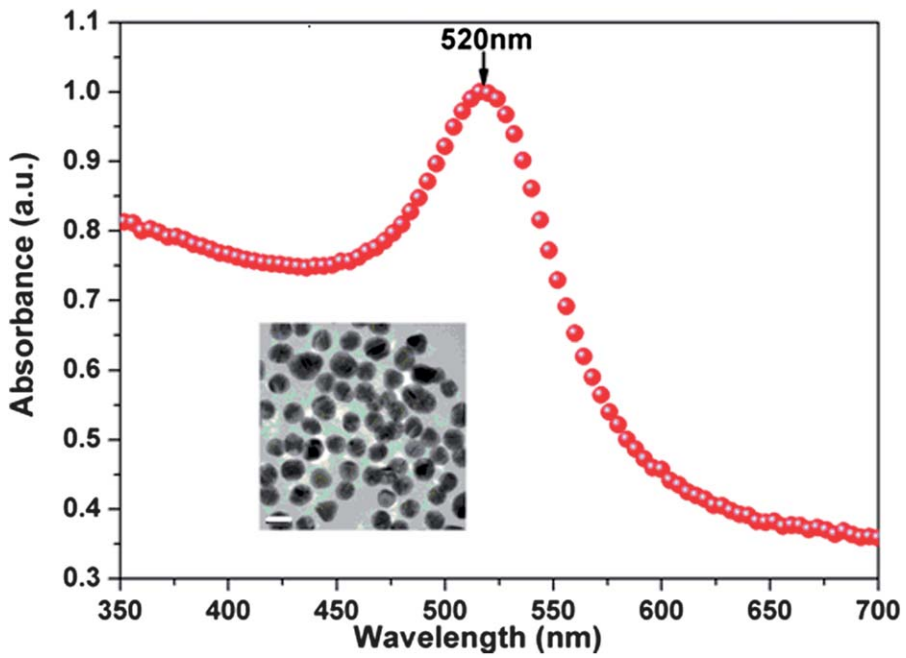

Fig. 2 Absorption spectrum of Au NPs in water. The inset is the TEM image of the NPs. The white bar is approximately 20 nm long.

ART ■ C1JM12820E

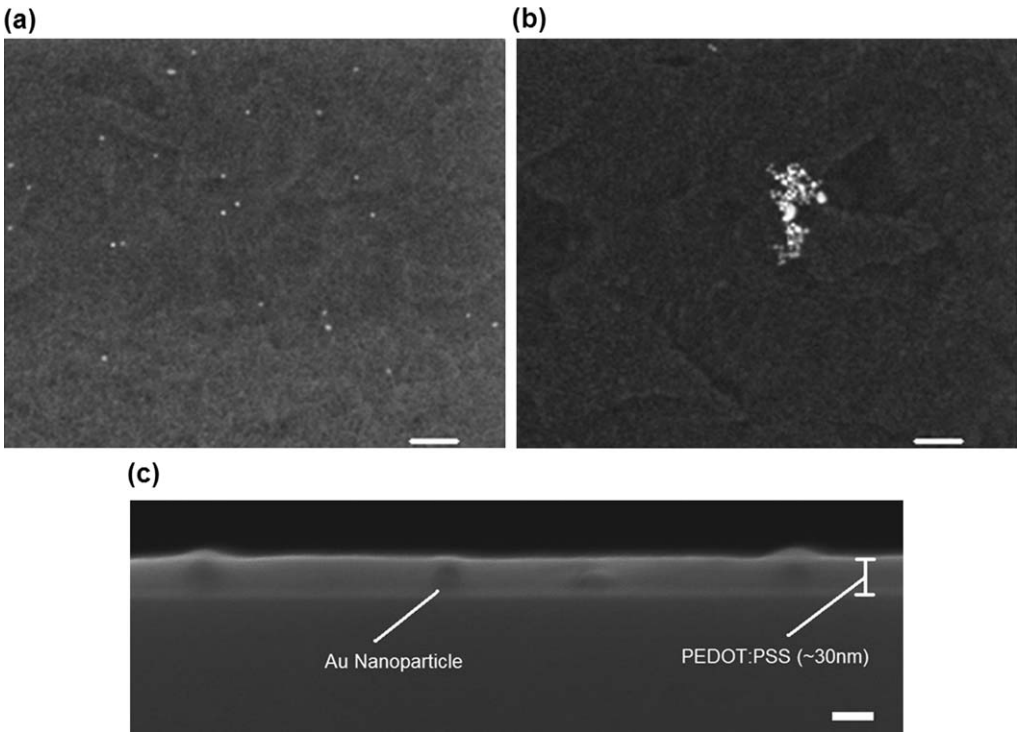

Fig. 3 SEM images of the surface of PEDOT:PSS:Au NP films with (a) Au NPs capped with PEG and (b) Au NPs not capped with PEG. The white bars in (a) and (b) are approximately 200 nm long. (c) SEM image of the cross-section of a PEDOT:PSS:Au NP film, with Au NPs capped with PEG. The white bar in (c) is approximately 30 nm long. Note that the image is focused on the cross-section surface of PEDOT:PSS and the Au NPs might be out of focus.

built a rigorous theoretical model to study the electromagnetic waves in the multilayered device structures, as shown in ESI A†. The theoretical enhancement factor (*i.e.* the ratio of the active-layer light absorption of the PEDOT:PSS:Au NP device to that of the conventional PEDOT:PSS one) shows no clear absorption enhancement, with a value around 1 as shown in the inset of Fig. 4a which agrees well with the experimental results. LSPR is at about 580 nm although the enhancement is weak. Our theoretical results and reflectance measurements also show that the Al electrode does not obviously affect the LSPR effect on the absorption enhancement as the Al electrode is situated far (220 nm) from the PEDOT:PSS layer.

The reason for the small optical enhancement is that when light is incident in normal into the device through ITO, the very strong near field around Au NPs due to LSPR mainly distributes laterally along the PEDOT:PSS layer rather than vertically into the adjacent active layer as shown in Fig. 5. As a result, no clear light absorption enhancement can be obtained in the active layer of P3HT:PCBM. Importantly, the understanding can also be applied to other cases with the metallic NPs (such as Ag, Pt, *etc.*) incorporated into the buffer layer adjacent to the active layer of typical organic thin-film solar cells due to the lateral distribution feature of the strong near-field. Meanwhile, the work suggests that near-field physics needs to be accounted for in the optical design of photovoltaics, and some traditional physical quantities, such as scattering cross section, are not enough to fully characterize the optical properties of PSCs. For instance, typically, the scattering cross-section is very useful to locate the plasmonic resonance region and determine the strength of scattering.[31,32] However, it cannot provide the directional properties of the electric field and thus the direction dependence of absorption enhancement.

Even though there is no obvious enhancement in the light absorption of the active layer, IPCE of our PEDOT:PSS:Au NP devices increases with the Au NP concentration and the 0.32 wt % device shows the highest IPCE, with ~64% at 550 nm as shown in Fig. 4b. For higher Au NP concentrations, IPCE decreases. This is in good agreement with the trend of J_{sc}. The apparent discrepancy between light absorption and IPCE can be explained by the fact that IPCE measures the percentage of incident photons that eventually results in free charges being collected through the PSC electrodes. Factors beyond light absorption, such as the resistance of electrodes, exciton dissociation rates and charge collection efficiencies, will also affect the magnitude of IPCE. However, such non-optical effects are likely to be not wavelength sensitive and are represented by vertical shifts of the entire IPCE spectrum. Comparing devices with or without Au NPs in Fig. 4b, we observe that our measured IPCE shows a wideband improvement from ~400 to 650 nm. We therefore conclude that electrical effects, instead of plasmonic effects, play a major role in performance improvement.

It should be noted that in the measurement of light absorption shown in Fig. 4a, we have eliminated the absorption of the PEDOT:PSS layer (with or without Au NPs) as it will absorb light. Therefore, the absorption spectrum represents light harvesting within the active layer only, which is important for understanding the plasmonic effects on device performances. The

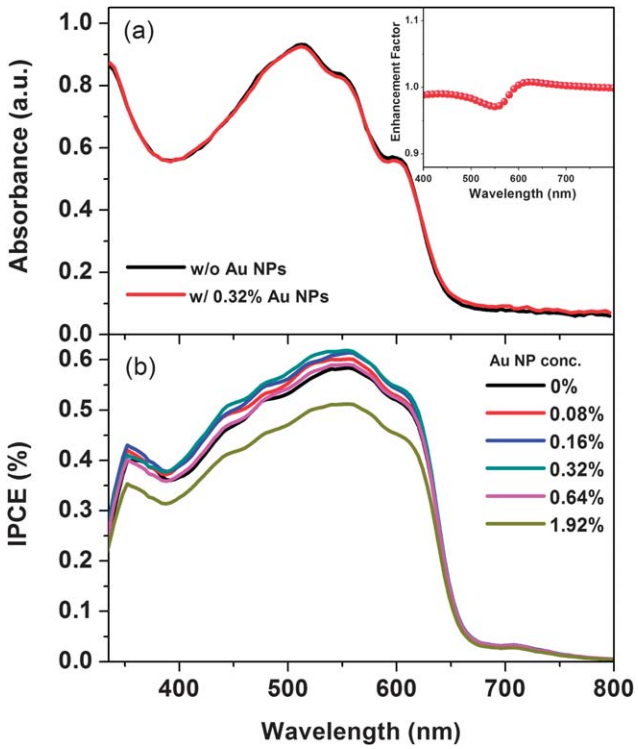

Fig. 4 (a) Absorbance of the PEDOT:PSS/P3HT:PCBM film with or without Au NP incorporation (0.32 wt%); the inset of (a) theoretical absorption enhancement factor (detailed model shown in ESI A†) and (b) IPCE of the solar cells with various Au NP concentrations in PEDOT:PSS.

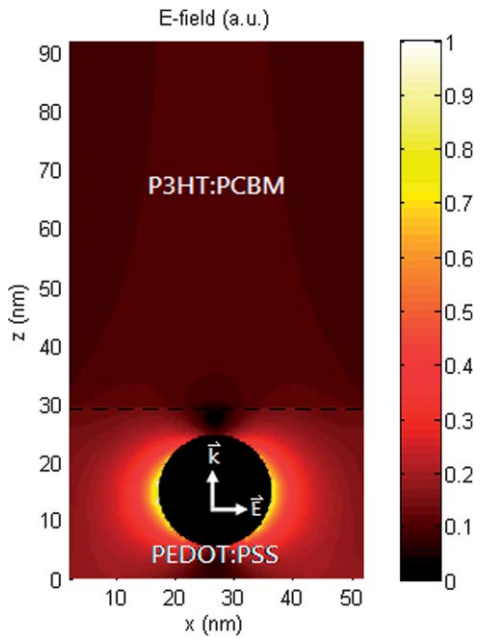

Fig. 5 Theoretical electric field profile in the PEDOT:PSS:Au NPs/P3HT:PCBM PSCs.

insignificant change in absorption spectra is a direct evidence that light absorption in P3HT:PCBM is unaffected by the incorporation of Au NPs.

3.4 Effects of Au NPs on PEDOT:PSS

The morphology changes of the PEDOT:PSS:Au NP layer are investigated by applying Atomic Force Microscopy (AFM) on a PEDOT:PSS:Au NP film for different NP concentrations as shown in Fig. 6. Upon increasing the Au NP concentration, we observed an obvious change in surface morphology of the PEDOT:PSS film, with an increase in roughness of ~5% and ~40% for 0.32 wt% and 0.64 wt% Au NPs, respectively. It has been reported that increasing anode surface roughness will increase the interface area between the anode and the active layer, providing shorter routes for holes to travel to the anode and enhancing hole collection at the anode.[33] The increased interfacial area between PEDOT:PSS and P3HT:PCBM allows the collection of a larger number of holes in the P3HT:PCBM layer, thus increasing J_{sc} of our devices. In addition, the reduced mean distance of between generated holes and the PEDOT:PSS interface diminishes the dependence of holes on the external electric field for collection at the anode, explaining the improvement in FF of our devices. Besides, it has been suggested that a rough P3HT:PCBM surface creates defect sites that assist exciton dissociation.[34] These effects together account for the improvements in J_{sc} and FF in our devices. In fact, we observe improved forward bias injection upon addition of Au NPs in our devices, further supporting our claim that the increased PEDOT:PSS roughness increases the PEDOT:PSS/P3HT:PCBM interfacial area (see ESI, Fig. S1†). Considering the optical effects of a rough PEDOT:PSS surface, we have measured the transmission of PEDOT:PSS with or without Au NPs and observed no discernible difference. In addition, the refractive index difference between PEDOT:PSS and P3HT:PCBM is not large and the roughness is in the nanoscale range. Hence, the rough PEDOT:PSS surface does not contribute to scatter light significantly (see ESI, Fig. S2†).

To further elucidate this effect, we have attempted to remove the surface roughness of the PEDOT:PSS layer while retaining Au NPs inside the PEDOT:PSS film. To accomplish this, an extra PEDOT:PSS layer is spin-coated on top of the PEDOT:PSS:Au NP layer. From our AFM images in Fig. 6, this extra layer smoothens the surface of the PEDOT:PSS to a morphology similar to a regular PEDOT:PSS layer. Devices are fabricated with the structure ITO/PEDOT:PSS:Au NPs/PEDOT:PSS/P3HT:PCBM/LiF (1 nm)/Al (100 nm). We observed that after the insertion of the pristine PEDOT:PSS layer, the presence of Au NPs in these devices provides no improvements in device performance (see ESI, Fig. S3†). Meanwhile, since optical effects have been proven to be unlikely to be a major contributor to performance improvement, one cannot argue that positive LSPR effects are diminished by the alteration of optical interference profile inside the PSC due to the addition of an extra layer of PEDOT:PSS. As a result, the main effect of the extra PEDOT:PSS layer is to smoothen the rough surface of the PEDOT:PSS:Au NP layer. Consequently, the results indicate that the rough PEDOT:PSS:Au NP layer surface positively contributes to device performances.

We also measured the resistance of PEDOT:PSS from resistive devices with the structure ITO/PEDOT:PSS:Au NPs/Al (80 nm). J–V measurements from these devices indicate a slight reduction in PEDOT:PSS resistance from 1.33 Ω (no NPs) to 0.97 Ω

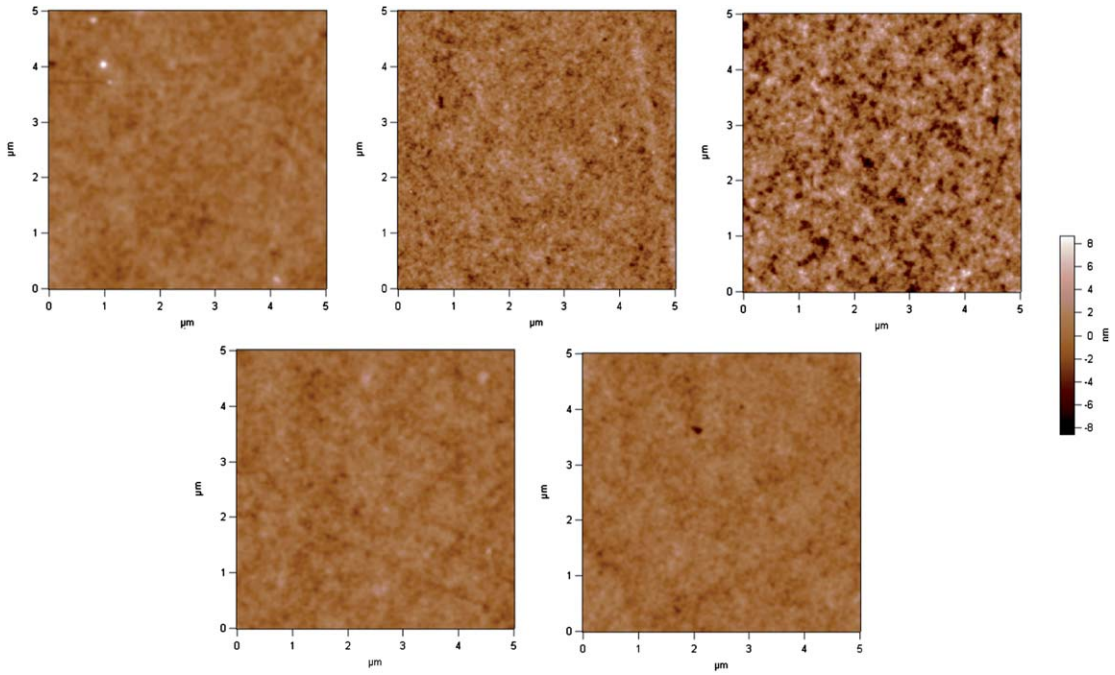

Fig. 6 AFM height images for different Au NP concentrations in PEDOT:PSS—0% (top left), 0.32% (top center), 0.64% (top right). After spin-coating an extra layer of PEDOT:PSS on top of the PEDOT:PSS:Au NP layer, the AFM images show a smoothened surface for 0.32% (bottom left) and 0.64% (bottom right).

(0.32 wt%). Although reduction in PEDOT:PSS resistance reduces the series resistance of PSCs, the small decrease in PEDOT:PSS resistance can only provide minor contributions to device performance improvement. On the whole, we conclude that the improved hole collection at the roughened interface between PEDOT:PSS and P3HT:PCBM enhances device performances, while a slight reduction in PEDOT:PSS resistance by the incorporation of Au NPs can also provide minor contribution to performance improvements.

3.5 Effects of Au NPs on exciton quenching

A missing picture is the origin of device performance degradation at high NP concentrations. To investigate this effect, we measured the photoluminescence (PL) spectrum of PEDOT:PSS: Au NPs/P3HT:PCBM films (see Fig. 7). The PL spectra show increasing PL intensity upon increasing concentrations of Au NPs, with a maximum of ~10% increase at ~647 nm.

PL intensity changes can be caused by three main reasons: changes in optical absorption, exciton quenching at metal/organic interfaces[35–37] and exciton quenching at donor/acceptor (D/A) interfaces.[38,39] The possibility of changes in optical absorption is eliminated, as we have experimentally and theoretically shown previously that light absorption of PSCs does not change significantly after incorporation of Au NPs. Considering the second reason, exciton quenching at metal/organic interfaces, it has been reported that capping an insulating layer on Au NPs can prevent direct contact between the metal and organic layer, hence preventing exciton quenching on the NP surface.[40] Furthermore, we have already shown in Fig. 3c that Au NPs located near the surface of PEDOT:PSS are well covered by PEDOT:PSS. Hence, we expect that the Au NPs are not in direct contact with the P3HT:PCBM layer and the effect of exciton quenching by Au NPs is negligible.

For the third reason, the reduction in exciton quenching at D/A junctions indicates reduced D/A interface area and hence a change in the morphology of the active layer.[41,42] We should be careful that studies have shown that the PL increase can be a result of an increase in crystallinity of P3HT in the P3HT:PCBM blend, causing an increase in hole mobility and PCE,[38,43,44] which apparently cannot address our results. However, it should be noted that the increase in crystallinity of P3HT has also been associated with an enhancement of

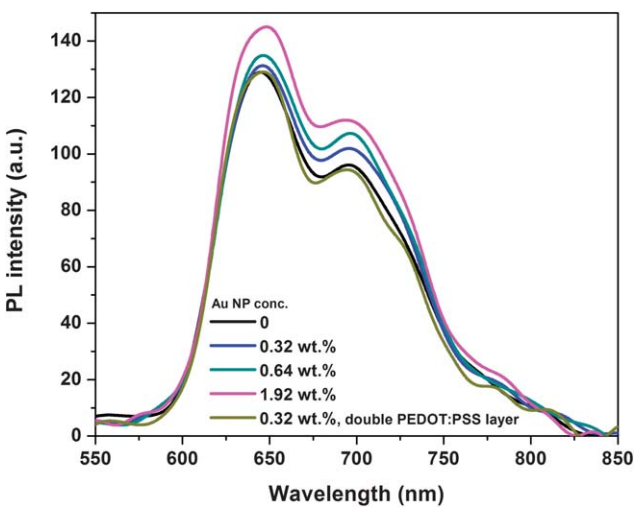

Fig. 7 Photoluminescence spectra of P3HT:PCBM for different Au NP concentrations in PEDOT:PSS.

absorption of P3HT:PCBM in the red region, which is not observed in our study. Hence, the increase in PL in our study is attributed to changes in phase separation in the P3HT:PCBM blend leading to the reduced D/A junction interfacial area, instead of changes in crystallinity of P3HT. The reduced D/A junction area causes exciton dissociation efficiency to decrease and reduces PCE. In fact, we also studied AFM images of the top surface of the P3HT:PCBM film and observed no significant change in top surface morphology (see ESI, Fig. S4†). This implies that the rough PEDOT:PSS surface, caused by the incorporation of NPs, could only cause a change in internal networking of the subsequently spin-coated P3HT:PCBM film near the PEDOT:PSS side.

To provide further evidence of the roughness effect on the change of phase separation, we measured the PL spectrum of the PEDOT:PSS:Au NPs/PEDOT:PSS/P3HT:PCBM film (see Fig. 7), and no significant difference in PL intensity between the samples with the single PEDOT:PSS layer (without Au NPs) and double PEDOT:PSS layer (with Au NPs in first layer) is observed. In this case, no clear PL intensity change is observed as the smoothened PEDOT:PSS surface, caused by the addition of an extra PEDOT:PSS layer, does not alter the internal networking of the active layer. Therefore, we conclude that incorporation of Au NPs modifies PEDOT:PSS surface morphology and leads to the reduced exciton quenching, which can be explained by alterations in the internal networking of the P3HT:PCBM film near the PEDOT:PSS side.

In terms of the impact on device performances, on one hand, the reduction in exciton quenching after addition of Au NPs implies a reduction in free carrier generation, leading to a lower J_{sc} and FF. On the other hand, the previously investigated hole collection improvement is advantageous to J_{sc} and FF. The competition between the two effects contributes to the trend in PCE variation as shown in Table 1: as Au NPs are added to PEDOT:PSS, the surface roughness increases, creating a larger PEDOT:PSS/P3HT:PCBM interface area. Therefore, more holes can be collected at the anode, leading to enhancements in J_{sc}, FF and PCE. However, the increased roughness also affects P3HT:PCBM networking and reduces exciton quenching. When the Au NP concentration increases further from 0.32% towards 1.92%, the negative effects of reduced exciton quenching outweigh the positive effects of improved hole collection, resulting in the reduction of PCE as shown in Table 1 and thus PCE peaks at 0.32 wt%.

4. Conclusions

In conclusion, we have demonstrated ~13% improvement in PCE for PSCs incorporating PEG-capped Au NPs in PEDOT:PSS, with enhancements mainly originating from J_{sc} and FF. A peak in PCE performance is obtained at an Au NP concentration of 0.32 wt%. The contribution of the LSPR effect to performance improvement has been investigated through rigorous modeling and experiment. Both theoretical and experimental results show that absorption enhancement due to incorporation of Au NPs is insignificant and provides only minor contribution to PCE improvement. We find that the reason is due to the lateral distribution feature of the strong near-field of plasmonic resonance around the metallic NPs. Importantly, the finding can also be applied to other cases with metallic NPs (such as Ag and Pt) incorporated into the buffer layer adjacent to active layers of typical organic thin film solar cells. Our work suggests that the optical properties of PSCs such as the direction dependence of absorption enhancement cannot be fully described by traditional physical quantities, such as scattering cross section. It is highly necessary to account for near-field physics in order to provide a full picture for the effective optical design of photovoltaics.

Considering electrical characteristics, we find that the incorporation of an appropriate amount of Au NPs reduces the resistance of the PEDOT:PSS layer. AFM images of NP incorporated PEDOT:PSS show that there is an increase in the interfacial roughness between P3HT:PCBM and PEDOT:PSS after incorporation of Au NPs. The roughened interface contributes to the improvement of hole collection efficiency and leads to J_{sc} and FF enhancements. PL measurements show that incorporation of Au NPs leads to reduced exciton quenching at D/A junctions at high NP concentrations due to the change in internal networking of the active layer. Our results indicate that the competition between the effects of hole collection improvements and reduced exciton quenching, instead of LSPR effects, leads to the performance peak at 0.32 wt%. This report highlights the importance of studying both optical and electrical properties for better understanding the origins of PCE improvements in PSCs incorporated with metallic NPs.

Acknowledgements

This work is supported by UGC grant (#400897) of the University of Hong Kong and the General Research Fund (HKU#712108 and HKU#712010) from the Research Grants Council of Hong Kong Special Administrative Region, China, financial support from Jiawei SolarChina, Co. Ltd. and a grant from the State Key Laboratory of Modern Optical Instrumentations (Zhejiang University). We also acknowledge Luminescence Technology Corp. for their materials at special prices. We acknowledge the useful discussion with W.C. Chew on the results of the work.

References

1 G. Dennler, M. C. Scharber and C. J. Brabec, *Adv. Mater.*, 2009, **21**, 1323–1338.
2 V. D. Mihailetchi, H. X. Xie, B. de Boer, L. J. A. Koster and P. W. M. Blom, *Adv. Funct. Mater.*, 2006, **16**, 699–708.
3 A. Yakimov and S. R. Forrest, *Appl. Phys. Lett.*, 2002, **80**, 1667–1669.
4 P. Peumans, A. Yakimov and S. R. Forrest, *J. Appl. Phys.*, 2003, **93**, 3693–3723.
5 P. E. Shaw, A. Ruseckas and I. D. W. Samuel, *Adv. Mater.*, 2008, **20**, 3516–3520.
6 P. W. M. Blom, V. D. Mihailetchi, L. J. A. Koster and D. E. Markov, *Adv. Mater.*, 2007, **19**, 1551–1566.
7 R. A. Pala, J. White, E. Barnard, J. Liu and M. L. Brongersma, *Adv. Mater.*, 2009, **21**, 3504–3509.
8 H. A. Atwater and A. Polman, *Nat. Mater.*, 2010, **9**, 205–213.
9 W. E. I. Sha, W. C. H. Choy and W. C. Chew, *Opt. Express*, 2010, **18**, 5993–6007.
10 W. E. I. Sha, W. C. H. Choy and W. C. Chew, *Opt. Lett.*, 2011, **36**, 478–480.
11 J. R. Cole and N. J. Halas, *Appl. Phys. Lett.*, 2006, **89**, 153120.
12 W. E. I. Sha, W. C. H. Choy, Y. P. Chen and W. C. Chew, *Opt. Express*, in press.
13 J. Weickert, R. B. Dunbar, H. C. Hesse, W. Wiedemann and L. Schmidt-Mende, *Adv. Mater.*, 2011, **23**, 1810–1828.

14 F.-C. Chen, J.-L. Wu, C.-L. Lee, Y. Hong, C.-H. Kuo and M. H. Huang, *Appl. Phys. Lett.*, 2009, **95**, 013305.
15 S.-S. Kim, S.-I. Na, J. Jo, D.-Y. Kim and Y.-C. Nah, *Appl. Phys. Lett.*, 2008, **93**, 073307.
16 B. P. Rand, P. Peumans and S. R. Forrest, *J. Appl. Phys.*, 2004, **96**, 7519–7526.
17 A. P. Kulkarni, K. M. Noone, K. Munechika, S. R. Guyer and D. S. Ginger, *Nano Lett.*, 2010, **10**, 1501–1505.
18 J. H. Lee, J. H. Park, J. S. Kim, D. Y. Lee and K. Cho, *Org. Electron.*, 2009, **10**, 416–420.
19 D. H. Wang, D. Y. Kim, K. W. Choi, J. H. Seo, S. H. Im, J. H. Park, O. O. Park and A. J. Heeger, *Angew. Chem., Int. Ed.*, 2011, **50**, 5519–5523.
20 C.-H. Kim, S.-H. Cha, S. C. Kim, M. Song, J. Lee, W. S. Shin, S.-J. Moon, J. H. Bahng, N. A. Kotov and S.-H. Jin, *ACS Nano*, 2011, **5**, 3319–3325.
21 W.-J. Yoon, K.-Y. Jung, J. Liu, T. Duraisamy, R. Revur, F. L. Teixeira, S. Sengupta and P. R. Berger, *Sol. Energy Mater. Sol. Cells*, 2010, **94**, 128–132.
22 K. Kim and D. L. Carroll, *Appl. Phys. Lett.*, 2005, **87**, 203113.
23 K. Topp, H. Borchert, F. Johnen, A. V. Tunc, M. Knipper, E. von Hauff, J. Parisi and K. Al-Shamery, *J. Phys. Chem. A*, 2009, **114**, 3981–3989.
24 M. Stavytska-Barba and A. M. Kelley, *J. Phys. Chem. C*, 2010, **114**, 6822–6830.
25 S. K. M. Jönsson, J. Birgerson, X. Crispin, G. Greczynski, W. Osikowicz, A. W. Denier van der Gon, W. R. Salaneck and M. Fahlman, *Synth. Met.*, 2003, **139**, 1–10.
26 B. V. Enüstün and J. Turkevich, *J. Am. Chem. Soc.*, 1963, **85**, 3317–3328.
27 J. Qian, L. Jiang, F. Cai, D. Wang and S. He, *Biomaterials*, 2011, **32**, 1601–1610.
28 C.-D. Wang and W. C. H. Choy, *Sol. Energy Mater. Sol. Cells*, 2011, **95**, 904–908.
29 F. Bouyer, A. Robben, W. L. Yu and M. Borkovec, *Langmuir*, 2001, **17**, 5225–5231.
30 A. S. Karakoti, S. Das, S. Thevuthasan and S. Seal, *Angew. Chem., Int. Ed.*, 2011, **50**, 1980–1994.
31 K. R. Catchpole and A. Polman, *Appl. Phys. Lett.*, 2008, **93**, 191113.
32 J.-Y. Lee and P. Peumans, *Opt. Express*, 2010, **18**, 10078–10087.
33 M.-H. Hsu, P. Yu, J.-H. Huang, C.-H. Chang, C.-W. Wu, Y.-C. Cheng and C.-W. Chu, *Appl. Phys. Lett.*, 2011, **98**, 073308.
34 G. Li, V. Shrotriya, Y. Yao and Y. Yang, *J. Appl. Phys.*, 2005, **98**, 043704.
35 L.-M. Chen, Z. Xu, Z. Hong and Y. Yang, *J. Mater. Chem.*, 2010, **20**, 2575–2598.
36 H. Becker, S. E. Burns and R. H. Friend, *Phys. Rev. B: Condens. Matter Mater. Phys.*, 1997, **56**, 1893.
37 D. E. Markov and P. W. M. Blom, *Phys. Rev. B: Condens. Matter Mater. Phys.*, 2005, **72**, 161401.
38 U. Zhokhavets, T. Erb, H. Hoppe, G. Gobsch and N. Serdar Sariciftci, *Thin Solid Films*, 2006, **496**, 679–682.
39 G. Li, V. Shrotriya, Y. Yao, J. Huang and Y. Yang, *J. Mater. Chem.*, 2007, **17**, 3126–3140.
40 H. Shen, P. Bienstman and B. Maes, *J. Appl. Phys.*, 2009, **106**, 073109.
41 M. Drees, H. Hoppe, C. Winder, H. Neugebauer, N. S. Sariciftci, W. Schwinger, F. Schaffler, C. Topf, M. C. Scharber, Z. Zhu and R. Gaudiana, *J. Mater. Chem.*, 2005, **15**, 5158–5163.
42 G. Li, Y. Yao, H. Yang, V. Shrotriya, G. Yang and Y. Yang, *Adv. Funct. Mater.*, 2007, **17**, 1636–1644.
43 Y. Kim, S. Cook, S. M. Tuladhar, S. A. Choulis, J. Nelson, J. R. Durrant, D. D. C. Bradley, M. Giles, I. McCulloch, C.-S. Ha and M. Ree, *Nat. Mater.*, 2006, **5**, 197–203.
44 H. Kim, W.-W. So and S.-J. Moon, *Sol. Energy Mater. Sol. Cells*, 2007, **91**, 581–587.

ART ■ C1JM12820E